Robotica (2014) volume 32, pp. 341–355. © Cambridge University Press 2013
doi:10.1017/S0263574713000696

Practical feasibility of a high-precision 3-UPU parallel mechanism

Gaurav Bhutani and T. A. Dwarakanath*

Division of Remote Handling and Robotics, Bhabha Atomic Research Centre, Mumbai 400085, India

(Accepted June 17, 2013. First published online: August 6, 2013)

SUMMARY
In this paper, we revisit the 3-degrees of freedom (DOF) pure translational mechanism. The mathematical model and the design considerations are discussed. A detailed sensitivity and error analysis is carried out and the results are discussed in a new perspective. The feasibility of the practical 3-DOF pure translational mechanism is established with novel design considerations to take care of theoretical mobility and geometrical constraints. We describe and validate the theoretical observations with stage-wise prototype models and experiments. The experimental results concur that all is well with 3-UPU in contrast to what is presented in refs. [6, 9, 10].

KEYWORDS: 3-UPU; Singularity analysis; Sensitivity analysis; Error analysis; Prototype development.

1. Introduction

Spatial 3-degree of freedom (DOF) pure translational mechanisms are mostly employed in the industry. Most of them are serial-based mechanisms and widely applied in three-axis cranes, machining centres, coordinate measuring machines, etc. Only recently, three-axis parallel mechanisms are making its entry in the industry through Delta robots in high-speed pick and place applications. The fully parallel mechanism exhibits high stiffness in most of the mechanism workspace.[1] There were interesting theoretical analyses,[1–5] which made a strong case for feasibility of simple and practical 3-DOF, fully parallel mechanisms and have come to be known as 3-UPU parallel mechanisms. The 3-UPU mechanism is the particular mechanism of the most generalized 3-RRPRR mechanism, wherein in the first and last, two individual revolute joints are replaced with universal joints, respectively. There are very few research reports based on experimental results. The observations and negative results presented in ref. [6] and a reference to this in a survey[7] raised the questions regarding the feasibility of a 3-UPU parallel mechanism. Later, it was shown that the geometry of UPU in ref. [6] is in singularity.[8] The research in refs. [9, 10] acknowledging the results of ref. [6] largely shifted the focus away from the UPU-based parallel mechanism. In an accuracy analysis with a joint clearance model given in ref. [9], the absolute sum of maximum of clearance taking up all of the individual joint pairs constituting the mechanism is a highly unlikely scenario. The model does not consider the effect of the geometry of the mechanism to arrive at the error at the output link. Adding the absolute values of the maximum errors in all the joints of the mechanism is an improper estimate and results in an unrealistically exaggerated value in a closed-loop mechanism. Going by the conflicting results between the theory and the observation based on the practical model, we chose to revisit the mechanism and build a theoretical model and validate it with stage-wise prototype models and experiments.

In this paper, we show that the 3-UPU mechanism proposed by Tsai and Joshi[1] can have an excellent practical feasibility. We show that there is no extreme kinematic sensitivity due to torsional clearances as it was projected to be in refs. [6, 9, 10]. We show the best limiting positions for prismatic joint actuation range, resolution of controllability in the reachable workspace and clearly demonstrate a singularity-free workspace. We arrive at the mechanism design solutions; we explain design steps to

* Corresponding author. E-mail: tad@barc.gov.in

take care of mechanism constraints. We show that with precise constraints and an accurate mechanism design, the prototype behaves as per the theoretical observations. We demonstrate various experiments to show the precision of the manipulator.

2. The 3-UPU Kinematic Structure

A simple kinematic analysis suggests that the mechanism based on the parallel architecture can possess high accuracy and repeatability. This is because the end-effector motion is generated by actuated links directly connected to the base. The simple kinematic analysis does not reveal the design challenges because of the high number of passive joints present in the mechanism. Therefore, the influence of passive joint selection or design has to be critically considered in a manipulator design. It is shown in ref. [2] that the 3-RRPRR, 3-DOF spatial parallel kinematic mechanism (SPKM) under some geometric conditions results in pure translational motion. Each of the three legs of the manipulator connected to the base through two revolute joints and the platform through two revolute joints has to meet the following conditions:

$$q_{i2} = q_{i4} \quad \text{and} \quad q_{i1} = q_{i5}, (i = 1, 2, 3), \tag{1}$$

where q_{i1} and q_{i2} are the unit vectors of passive revolute joint axes at the base and, similarly, q_{i4} and q_{i5} are the unit vectors of passive revolute joint axes at the platform. When the assembly of the base is made, the three legs and the platform should be under the following geometrical conditions.

Figures 1 and 2 show a kinematic sketch and describe the manipulator parameters. The three base connection points are chosen to form an equilateral triangle and so are the connection points at the platform. The coordinates of all the points are defined with respect to a global coordinate system fixed at the geometrical centre of the base **O**(*XYZ*) as shown in Figs. 1 and 2. The above straightforward choice is based on the symmetry. The plane formed by the connection points at the platform is parallel to the base. The height of the manipulator is described as the normal distance from the base to the platform plane. Let b be the side of the base equilateral triangle and a be the side of the platform equilateral triangle. Note that l_1, l_2, l_3 are the leg lengths connecting the base connector point B_i to the corresponding platform point A_i; $i = 1, 2, 3$. $\hat{i}$, $\hat{j}$, $\hat{k}$ are the unit vectors along the **X**, **Y** and **Z** axes; $(x, y, z)^T$ are the coordinates of the centre of the platform from **O**(*XYZ*). The coordinates of the leg connection points at the base and the platform with respect to **O**(*XYZ*) are given by

$$B_1 = \left[\frac{b}{\sqrt{3}}, 0, 0\right]^T, \quad B_2 = \left[\frac{-b}{2\sqrt{3}}, \frac{b}{2}, 0\right]^T, \quad B_3 = \left[\frac{-b}{2\sqrt{3}}, \frac{-b}{2}, 0\right]^T.$$

$$A_1 = \left[\frac{a}{\sqrt{3}} + x, y, z\right]^T, \quad A_2 = \left[\frac{-a}{2\sqrt{3}} + x, \frac{a}{2} + y, z\right]^T, \quad A_3 = \left[\frac{-a}{2\sqrt{3}} + x, \frac{-a}{2}, y, z\right]^T.$$

The three leg vectors from the base connection points to the platform connection points are

$$\vec{l}_1 = \vec{A}_1 - \vec{B}_1; \quad \vec{l}_2 = \vec{A}_2 - \vec{B}_2; \quad \vec{l}_3 = \vec{A}_3 - \vec{B}_3. \tag{2}$$

The inverse kinematics solution can be written as

$$\left(\frac{a}{\sqrt{3}} - \frac{b}{\sqrt{3}} + x\right)^2 + y^2 + z^2 = l_1^2, \tag{3}$$

$$\left(\frac{b}{2\sqrt{3}} - \frac{a}{2\sqrt{3}} + x\right)^2 + \left(\frac{a}{2} - \frac{b}{2} + y\right)^2 + z^2 = l_2^2, \tag{4}$$

$$\left(\frac{b}{2\sqrt{3}} - \frac{a}{2\sqrt{3}} + x\right)^2 + \left(\frac{b}{2} - \frac{a}{2} + y\right)^2 + z^2 = l_3^2. \tag{5}$$

https://doi.org/10.1017/S0263574713000696 Published online by Cambridge University Press

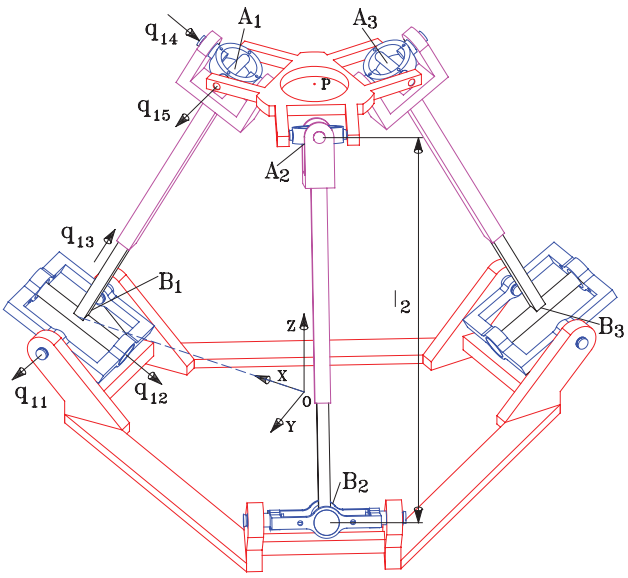

Fig. 1. (Colour online) Three-DOF SPKM.

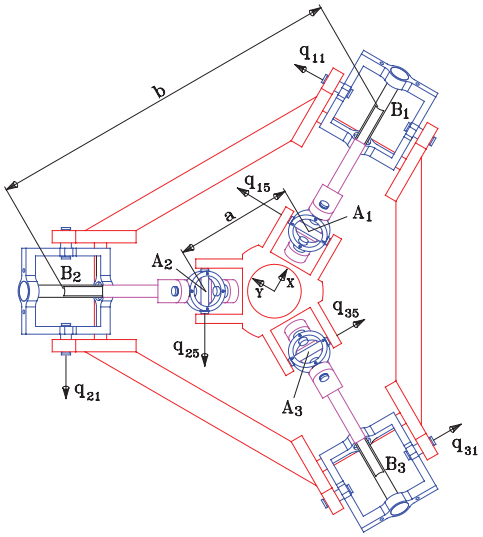

Fig. 2. (Colour online) Top view of SPKM to describe kinematic parameters.

3. Singularity and Sensitivity Analysis

There can be a point and a region around it in the workspace where the performance can be classified as the best and is the preferred region for the manipulator operations. The sensitivity analysis is to identify such regions and in general to understand how the sensitivity varies from point to point within a workspace of a manipulator. The sensitivity is defined as the ratio of the rate of change of leg lengths to the rate of change of motion of the platform. The Eq. (6) gives the transmission ratio of the velocities of the legs and the platform using combined Jacobian, J.[11] It is modified to reveal the transmission sensitivity

$$i = Jv_p \quad \Rightarrow \quad dl = Jdr, \tag{6}$$

where $i = [i_1, i_2, i_3]^T$ and $v_p = [\dot{x}, \dot{y}, \dot{z}]^T$ are the active leg velocities and the platform velocity, respectively. $dl = [dl_1, dl_2, dl_3]^T$ and $dr = [dx, dy, dz]^T$ are infinitesimal change in active leg lengths and the corresponding change in the platform position. The elements of J can be obtained by differentiating the inverse kinematic equations (3), (4) and (5). The relation in the matrix form is

https://doi.org/10.1017/S0263574713000696 Published online by Cambridge University Press

given as

$$\begin{bmatrix} dl_1 \\ dl_2 \\ dl_3 \end{bmatrix} = \begin{bmatrix} \frac{1}{l_1}\left(\frac{a}{\sqrt{3}} - \frac{b}{\sqrt{3}} + x\right) & \frac{1}{l_1}y & \frac{1}{l_1}z \\ \frac{1}{l_2}\left(\frac{b}{2\sqrt{3}} - \frac{a}{2\sqrt{3}} + x\right) & \frac{1}{l_2}\left(\frac{a}{2} - \frac{b}{2} + y\right) & \frac{1}{l_2}z \\ \frac{1}{l_3}\left(\frac{b}{2\sqrt{3}} - \frac{a}{2\sqrt{3}} + x\right) & \frac{1}{l_3}\left(\frac{b}{2} - \frac{a}{2} + y\right) & \frac{1}{l_3}z \end{bmatrix} \begin{bmatrix} dx \\ dy \\ dz \end{bmatrix}. \tag{7}$$

The sensitivity indices are given by the members of the 3×3 Jacobian matrix. The nine sensitivity indices are $\frac{dl_1}{dx}, \frac{dl_1}{dy}, \frac{dl_1}{dz}, \frac{dl_2}{dx}, \frac{dl_2}{dy}, \frac{dl_2}{dz}, \frac{dl_3}{dx}, \frac{dl_3}{dy}, \frac{dl_3}{dz}$. The absolute range of sensitivity of the leg is from zero to one. Zero being no participation of the leg in the direction of the translation of the platform at the point and one being the maximum participation of the leg in concerned motion of the platform. Also, for non-singular motion, not all the three legs can have the sensitivity of either zero or one at the same point for a particular direction of motion of the platform. Isotropy in sensitivity (or equal participation of all the legs) is a most sought after quality but the sensitivity is not isotropic at all points in the workspace. The sensitivity analysis is to determine how the sensitivity would vary in the space to perform the input range synthesis. The sensitivity is a function of proportion of the manipulator parameters. The size of the base, the size of the platform and the spatial location of the platform constitute the parameter set. The sensitivity indices are obtained as a function of manipulator parameters and the best sensitivity indices for a set of points (workspace) can be known. In this section, the mathematical model is developed for the sensitivity analysis of a 3-DOF SPKM. A numerical example considering the realistic values of the manipulator parameters of the prototype is given. In the later section, we also give the details of the prototype development based on the numerical values given in the example and discuss the experimental results.

3.1. Sensitivity with respect to an arbitrary displacement vector

The sensitivity index of a leg with respect to an arbitrary displacement vector $d\vec{r}$ is computed. The position vector of the platform with respect to $\mathbf{O}(XYZ)$ is given by

$$\vec{r} = x\hat{\imath} + y\hat{\jmath} + z\hat{k}. \tag{8}$$

Differentiating the above, the displacement vector of the platform is written as

$$d\vec{r} = dx\hat{\imath} + dy\hat{\jmath} + dz\hat{k}. \tag{9}$$

From the previous subsection, the arbitrary leg vector is of the form

$$\vec{l}_i = (x + c_{i1})\hat{\imath} + (y + c_{i2})\hat{\jmath} + (z + c_{i3})\hat{k}, \tag{10}$$

$$l_i^2 = (x + c_{i1})^2 + (y + c_{i2})^2 + (z + c_{i3})^2, \tag{11}$$

where $c_{i1}, c_{i2}, c_{i3}, i = 1, 2, 3$ are constants for a manipulator. Differentiating Eqn. (11), we have

$$l_i dl_i = (x + c_{i1})dx + (y + c_{i2})dy + (z + c_{i3})dz = \vec{l}_i \cdot d\vec{r}. \tag{12}$$

The sensitivity index with arbitrary displacement vector, $d\vec{r}$, is given by

$$\frac{dl_i}{dr} = \frac{\vec{l}_i \cdot d\vec{r}}{l_i dr} = \hat{l}_i \cdot d\hat{r} = \cos\theta, \tag{13}$$

where $\hat{l}_i$ is a unit vector along $\vec{l}_i$, $d\hat{r}$ is a unit vector along $d\vec{r}$, and θ is the angle between $\vec{l}_i$ and $d\vec{r}$. The sensitivity index is given by the dot product of the unit leg vector and the unit displacement vector and therefore is equal to cosine of the angle between them. For illustration, dl_1/dx is given by the cosine of the angle between $\vec{l}_1$and the X axis. For the motion of the platform along the Z axis, the absolute

https://doi.org/10.1017/S0263574713000696 Published online by Cambridge University Press

value of the cosine of the angle between $\vec{l}_1$ and the X axis decreases and hence dl_1/dx decreases. The expression also implies that the change in the leg length is always less than or equal to the resultant distance traversed by the platform of the SPKM. A synthesis of the manipulator workspace based on *dl/dr* is a tradeoff between fine control resolution, and a high motion response.

3.2. Isotropic sensitivity for three legs

The isotropic sensitivity of the three legs for a given displacement vector at a point in the workspace is important. In other words, it is important to find a translation vector from a point in the workspace, wherein the sensitivities of all the three legs are equal. The *isotropic* sensitivity equation can be written as $\hat{l}_1 \cdot d\hat{r} = \hat{l}_2 \cdot d\hat{r} = \hat{l}_3 \cdot d\hat{r}$. From Eqs. (9), (10) and (13), the expressions for $\hat{l}_i \cdot d\hat{r}$, $i = 1,2,3$ are obtained. Equating the three expressions, we get

$$\frac{1}{l_1}\left[\left(\frac{a}{\sqrt{3}} - \frac{b}{\sqrt{3}} + x\right)dx + ydy + zdz\right] = \frac{1}{l_2}\left[\left(\frac{b}{2\sqrt{3}} - \frac{a}{2\sqrt{3}} + x\right)dx + \left(\frac{a}{2} - \frac{b}{2} + y\right)dy + zdz\right] = \frac{1}{l_3}\left[\left(\frac{b}{2\sqrt{3}} - \frac{a}{2\sqrt{3}} + x\right)dx + \left(\frac{b}{2} - \frac{a}{2} + y\right)dy + zdz\right].$$

The above equation can be solved in two ways. In the first case, the position of the centre of the platform with respect to $\mathbf{O}(XYZ)$ is taken to be known. That is, $\vec{r} = x\hat{i} + y\hat{j} + z\hat{k}$ is known, and we calculate the unit displacement vector $\frac{d\vec{r}}{r} = \frac{dx\hat{i}+dy\hat{j}+dz\hat{k}}{r}$. The equations formed would be a set of linear equations giving a single solution. In the second case, we take the unit displacement vector to be given, $\frac{d\vec{r}}{r} = \frac{dx\hat{i}+dy\hat{j}+dz\hat{k}}{r}$, and we determine the position of the platform, $\vec{r} = x\hat{i} + y\hat{j} + z\hat{k}$, in the workspace. The equations formed would be a set of non-linear equations giving multiple solutions for this problem. The set of equations for the first case is

$$\left[\frac{1}{l_1}\left(\frac{a}{\sqrt{3}} - \frac{b}{\sqrt{3}} + x\right) - \frac{1}{l_2}\left(\frac{b}{2\sqrt{3}} - \frac{a}{2\sqrt{3}} + x\right)\right]\frac{dx}{dz} + \left[\frac{1}{l_1}y - \frac{1}{l_2}\left(\frac{a}{2} - \frac{b}{2} + y\right)\right]\frac{dy}{dz} + z\left(\frac{l_2 - l_1}{l_2 l_1}\right) = 0,$$

$$\left[\frac{1}{l_1}\left(\frac{a}{\sqrt{3}} - \frac{b}{\sqrt{3}} + x\right) - \frac{1}{l_3}\left(\frac{b}{2\sqrt{3}} - \frac{a}{2\sqrt{3}} + x\right)\right]\frac{dx}{dz} + \left[\frac{1}{l_1}y - \frac{1}{l_3}\left(\frac{b}{2} - \frac{a}{2} + y\right)\right]\frac{dy}{dz} + z\left(\frac{l_3 - l_1}{l_3 l_1}\right) = 0.$$

Considering the symmetry at $x = 0$, $y = 0$, and expressing the leg length in terms of manipulator parameters, we get

$$l_1 = l_2 = l_3 = \sqrt{\left(\frac{a}{\sqrt{3}} - \frac{b}{\sqrt{3}}\right)^2 + z^2}.$$

Substituting the above values and solving the equations, we get $\frac{dx}{dz} = \frac{dy}{dz} = 0$,

$$\frac{d\vec{r}}{r} = \frac{0\hat{i} + 0\hat{j} + dz\hat{k}}{dz} = \hat{k}.$$

The result states that if the translation is along the Z axis (at $x = 0$, $y = 0$), the sensitivity of the three legs is equal and therefore any point on the Z axis is isotropic.

3.3. Variation of sensitivity indices in manipulator workspace

An SPKM having design parameters $b = 329$, $a = 78$, $159 \leq l_i \leq 245$, based on which the prototype is developed, is considered to characterize sensitivity at various points in the workspace. The sensitivity parameters at various points inside the workspace are computed. Figure 3 shows the distribution of leg

https://doi.org/10.1017/S0263574713000696 Published online by Cambridge University Press

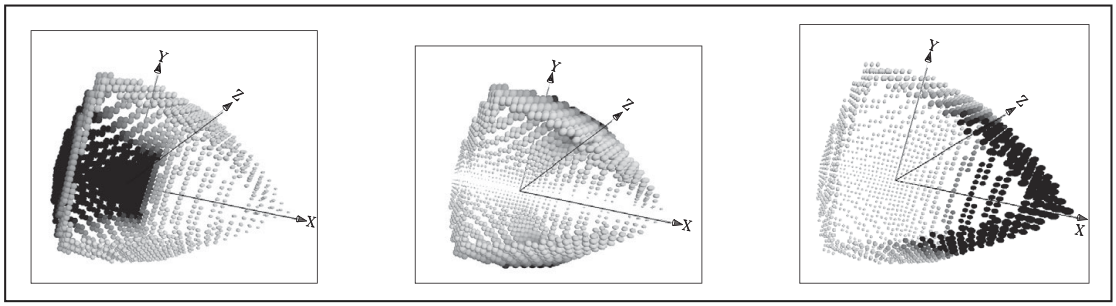

Fig. 3. Leg sensitivity distribution, $dl_1/dx, dl_1/dy, dl_1/dx$, on workspace envelope due to positional change along the *X, Y* and *Z* axes, respectively.

sensitivity $dl_1/dx, dl_1/dy, dl_1/dz$ on workspace envelopes. It represents only the relative variation of the sensitivity parameters. Because of the symmetry, the distribution of leg sensitivities of other two legs is same as in Fig. 3. The shade of the sphere represents the value of the sensitivity parameter. The darker shade on the envelopes represents the high sensitivity or high control resolution and the lighter shade represents smaller sensitivity or higher motion response. The envelopes always exhibit extremities of sensitivity range.

The extreme sensitivities would always be at the envelopes of the workspace. The magnitude of leg sensitivity at a point and its distribution in the manipulator workspace not only give good insight in planning the fine control resolution trajectories in task space but also give a good handle to design a right balance between control resolution and motion response. The size of the spheres indicates the sensitivity, while the sparseness of the spheres indicates the motion response.

3.4. Singularity-free workspace

The singularity-free workspace and kinematic synthesis are important to set the boundaries of the workspace farthest from singularities. The mechanism will have an undesirable mobility at or near singular positions due to poor stiffness along one or more directions. The singularity aspect of 3-UPU is well presented in earlier work.[5] The singularity analysis pertaining to the numerical values of the design parameters, based on which the prototype is built, is presented. The numerical values of the kinematic parameters are $b = 329$, $a = 78$, and prismatic stroke range of $159 \leq l_i \leq 245$ $(i = 1, 2, 3)$.

The singularity occurs under any of the following three conditions:

(1) Rotational singularity, when $\hat{n}_1 \cdot (\hat{n}_2 \times \hat{n}_3) = 0$, where $\hat{n}_1 = (\hat{q}_{i1} \times \hat{q}_{i2})$.
(2) Translation singularity, when the scalar triple product $\hat{l}_1 \cdot (\hat{l}_2 \times \hat{l}_3) = 0$.
(3) The other condition for translation singularity is when, $(n_i \cdot \hat{l}_i) = 0$.

Condition (1) results in a cylindrical singularity surface;[5] the diameter of the cylinder is 578.412 for the chosen numerical kinematic parameters. Conditions (2) and (3) occur when the platform is in coplanar with the base. Even with above three singularity constraints, the feasible design space is quite large. The design space is considerably reduced by symmetric considerations, the kinematic arrangement is designed tri-symmetric with respect to the global *Z* axis, the workspace boundary surfaces lie at equal distances from singular surfaces. The synthesis of the proportion of design parameters and practical ranges for active prismatic strokes is arrived so as to remain farthest from singular surfaces. Figure 4 shows the secure separation of workspace from cylindrical singularity surface and Fig. 5 shows the safe distance from the platform getting coplanar with the base, the distance of separation is represented by the vertical line. The mechanism would be in singularity if the reference point of the platform coincides with any point on the cylindrical singularity surface shown in Fig. 6. Six positions of the platform out of infinite singular configurations are shown in Fig. 6. It is shown that these positions lie outside and far away from the actual reachable workspace of the platform (see Figs. 4 and 5).

https://doi.org/10.1017/S0263574713000696 Published online by Cambridge University Press

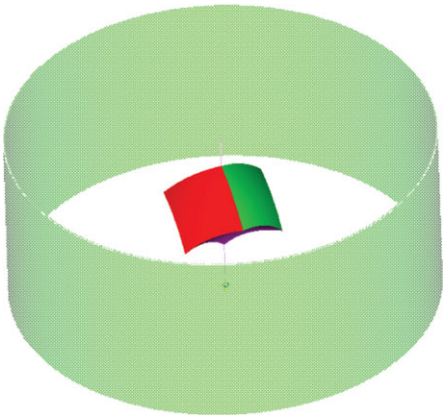

Fig. 4. (Colour online) Positioning of workspace relative to singular surface.

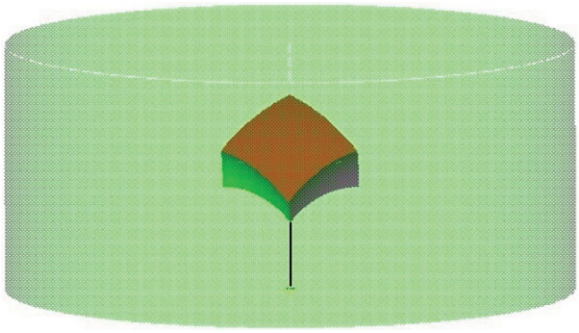

Fig. 5. (Colour online) Separation of workspace relative to base surface of singularity.

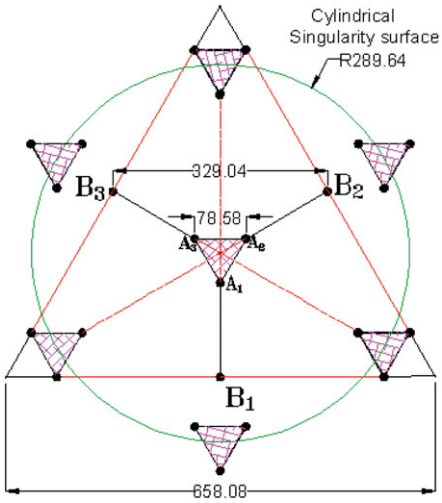

Fig. 6. (Colour online) Position of platform at home position and six singular configurations.

4. Error Analysis

In this section, we will analyse the torsional joint clearance errors and its influence on the posture accuracy of the platform. The major source of error is torsional rotation in universal joints. The design parameters of the manipulator are known. The geometrical arrangement of the leg as well as the platform is set to satisfy the geometric conditions given in Eq. (1). The home posture is defined when the platform (the plane formed by the three connection points at the platform) is parallel to the base and the prismatic joint axis of the each connector is normal to both the axes of the universal joints on the either side.

https://doi.org/10.1017/S0263574713000696 Published online by Cambridge University Press

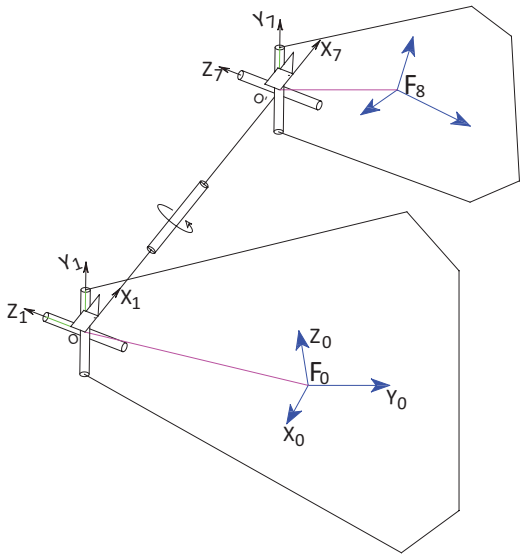

Fig. 7. (Colour online) Description of joint frames of UPU at home position for the purpose of error analysis.

The home posture is set, when the legs are at the minimum length and the x and y coordinates are zero. At the home posture, the passive rotations of the universal joints as well as the torsional rotations are taken as zero. In other words, the home posture serves as the reference for all the passive rotations as well as torsional rotation measurement. The posture of the platform coordinate frame, F_8, is assumed to be given with respect to base coordinate frame, F_0. The inverse kinematic solution is easily obtained and the leg lengths l_1, l_2, l_3 can be found. A mathematical model is obtained to formulate a matrix equation relating the posture of the platform to passive joint rotations of the 3-UPU and an additional torsional rotation about each of the prismatic axis. We solve for all the 12 rotations of all the joints of 3-UPU as well as three additional torsional rotations about the prismatic axis for a given posture of the platform. It is important to know the torsional rotations of passive joints for the given posture of the platform. Thereby, one can find out the extent of torsional mobility required to satisfy the posture. To set up a model, a coordinate frame is defined in each of the body separated by the joints. The frames are numbered from the base to the platform progressively and the frame n is termed as F_n. F_0 is the fixed frame attached to the geometrical centre of the base. F_1 is attached to leg connection point at the base. The position and orientation of the frame, n, with respect to the preceding frame, m, are described by the DH parameters, the homogeneous transformation matrix is given by ${}^{m}_{n}T$. F_7 is attached to leg connection point at platform and F_8 is attached to the geometrical centre of the platform as shown in the Fig. 7. Rest of the frames, $F_2 \ldots . F_6$, are attached at the intermediate bodies of the connector.

${}^{0}_{1}T$ is the transformation of F_1 with respect to fixed F_0. ${}^{7}_{8}T$ is the transformation of F_8 with respect to F_7. The connecting points at the base and at the platform are known in F_0 and F_8, respectively.

The other intermediate frames and their successive transformations are as given below:

(1) ${}^{1}_{2}T$: Rotation θ_1 of F_2 with respect to F_1 about Y_1 (Passive rotation due to universal Joint).
(2) ${}^{2}_{3}T$: Rotation θ_2 of F_3 with respect to F_2 about Z_2 (Passive rotation).
(3) ${}^{3}_{4}T$: Rotation θ_3 of F_4 with respect to F_3 about X_3 axes (Torsional backlash error).
(4) ${}^{4}_{5}T$: Translation of F_5 with respect to F_4 along X_4 axes (Prismatic joint).
(5) ${}^{5}_{6}T$: Rotation θ_5 of F_6 with respect to F_5 about Z_5 axes (Passive rotation).
(6) ${}^{6}_{7}T$, Rotation θ_6 of F_7 with respect to F_6 about Y_6 axes (Passive rotation).

We solve analytically for all the passive joint rotations and torsional rotations for the three connectors for a given platform posture. The solution gives insight into the mobility of the passive joints for a given posture. The results are presented in Tables I–V. The following tables give platform posture followed by corresponding mobility of all the passive and torsional rotations for one connector.

https://doi.org/10.1017/S0263574713000696 Published online by Cambridge University Press

Table I. Platform at home posture.

Rotation along X	Rotation along Y	Rotation along Z	Translation along X	Translation along Y	Translation along Z
0	0	0	0	0	100
			Joint space vector		
	θ_1 (Passive)	θ_2 (Passive)	θ_3 (Error)	θ_5 (Passive)	θ_6 (Passive)
Leg 1	0	0	0	0	0
Leg 2	0	0	0	0	0
Leg 3	0	0	0	0	0

Table II. Parallel to base posture and translation along the Z axis.

Rotation along X	Rotation along Y	Rotation along Z	Translation along X	Translation along Y	Translation along Z
0	0	0	0	0	150
			Joint space vector		
	θ_1 (Passive)	θ_2 (Passive)	θ_3 (Error)	θ_5 (Passive)	θ_6 (Passive)
Leg 1	8.95°	0	0	0	−8.95°
Leg 2	8.95°	0	0	0	−8.95°
Leg 3	8.95°	0	0	0	−8.95°

Table III. Rotation about the X axis.

Rotation along X	Rotation along Y	Rotation along Z	Translation along X	Translation along Y	Translation along Z
5°	0	0	0	0	100
			Joint space vector		
	θ_1 (Passive)	θ_2 (Passive)	θ_3 (Error)	θ_5 (Passive)	θ_6 (Passive)
Leg 1	0	0	−2.5°	5°	0
Leg 2	−0.98°	−0.045°	1°	2.2°	5.2°
Leg 3	−1.19°	−0.045°	1.4°	2.1°	5.5°

Table IV. Rotation about the Y axis.

Rotation along X	Rotation along Y	Rotation along Z	Translation along X	Translation along Y	Translation along Z
0	5°	0	0	0	100
			Joint space vector		
	θ_1 (Passive)	θ_2 (Passive)	θ_3 (Error)	θ_5 (Passive)	θ_6 (Passive)
Leg 1	1.11°	0°	0°	0°	−6.1°
Leg 2	0.66°	0.04°	2.3°	−3.7°	−3.25°
Leg 3	0.66°	0.04°	−2.3°	3.7°	3.25°

Tables I–V show the passive and torsional rotations required for the given postures of the platform. It can be observed from the tables that the rotation of the platform always results in torsional rotation (θ_3) of the connector. For a pure translational designated 3-UPU manipulator, the combined torsional stiffness of the connectors dictates the rotational stiffness of the manipulator. The results in Tables I–V also give the required mobility range in U–U joints for the desired workspace. Figure 8 shows the concurrent torsional rotations (θ_3) in all the three connectors for the various rotation of the platform about the Z axis. Further, for a constant torsional mobility of the platform, the required concurrent torsional rotation (θ_3) of connectors for various Z translations is studied. Figure 9 shows the required amount of concurrent torsional play (θ_3) of connectors for increasing Z translations for constant torsional play of 2.5° of the platform. It can be observed that at smaller Z translations, the torsional mobility of the platform has higher sensitivity to θ_3 but flatten out at after certain Z translation, the

https://doi.org/10.1017/S0263574713000696 Published online by Cambridge University Press

Table V. Rotation about the Z axis.

Rotation along X	Rotation along Y	Rotation along Z	Translation along X	Translation along Y	Translation along Z
0	0°	5°	0	0	100
			Joint space vector		
	θ_1 (Passive)	θ_2 (Passive)	θ_3 (Error)	θ_5 (Passive)	θ_6 (Passive)
Leg 1	−0.094°	2.49°	4.34°	−5°	−0.25°
Leg 2	0.094°	−2.49°	4.34°	5°	0.25°
Leg 3	−0.094°	2.49°	4.34°	−5°	−0.25°

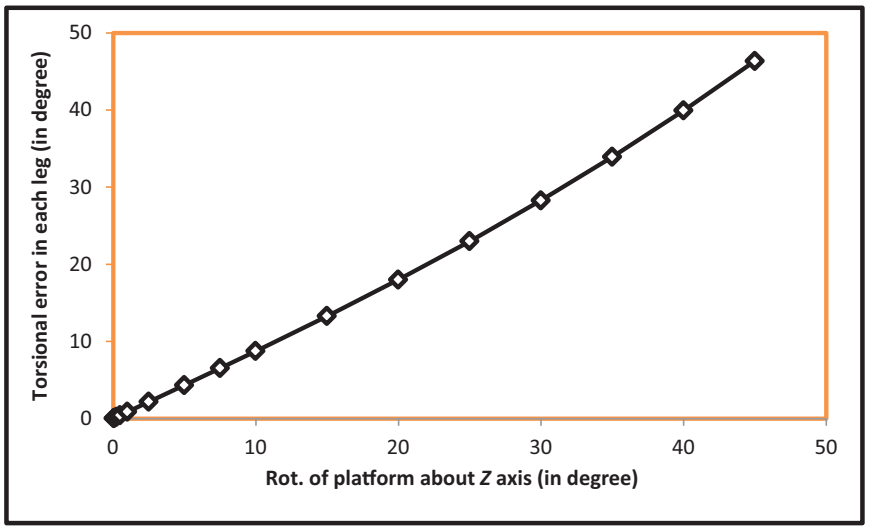

Fig. 8. (Colour online) Proportionality in torsional error.

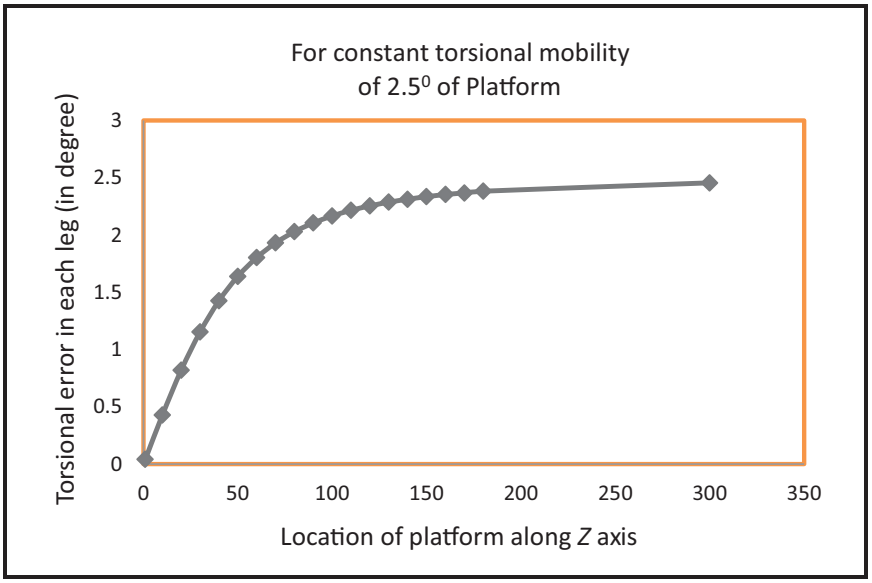

Fig. 9. (Colour online) Concurrent torsional rotation, (θ_3), of connectors for increasing Z translations at constant torsional mobility of 2.5° of platform.

https://doi.org/10.1017/S0263574713000696 Published online by Cambridge University Press

result serves to design the Z translation range. The main conclusion from the above analysis is that there is no extreme kinematic sensitivity to the torsional errors within the certain working range of the manipulator. The above analysis serves to plan the working range of the manipulator. Clearly, the presence of torsional clearances concurrently in more than one connector will result in unwanted proportional rotational mobility on the platform.

5. Design Consideration, Prototype Development and Experiments

In this section, we present the engineering design considerations to achieve very closely what is recommended in a theoretical kinematic design. Therefore, the design steps, which establish and maintain the geometric conditions, are very important.[12] Two universal joints, each built with common cube block with a pair of orthogonal hinges located closely together, seem to be a straightforward solution but for the torsional backlash. As shown in the previous section, the presence of torsional backlash will influence the rotational mobility of the manipulator platform. The universal joints are meant to transmit high torque with minimal direction reversals and not for establishing high-precision geometric constraints. A small clearance along the radial direction and close hinge supports would ill-define a hinge axis, whereas with the same clearance but with the longer bearing support would considerably reduce the angular play. Figures 10 and 11 show this in an exaggerated fashion.

We further studied this aspect by building a 3-UU structure based on single block universal joints. The prototype is shown in Fig. 12. The platform motions are measured and it is found to be much less

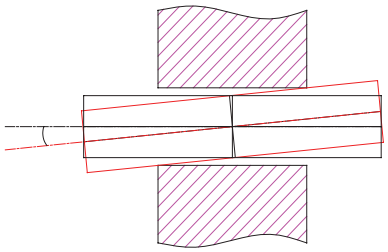

Fig. 10. (Colour online) Shorter bearing supports higher angular play.

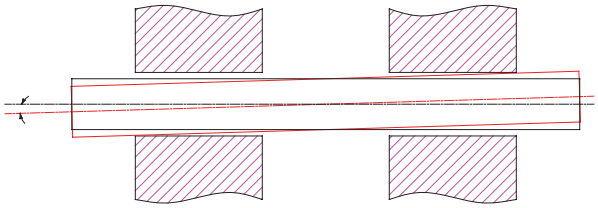

Fig. 11. (Colour online) Longer bearing supports smaller angular play.

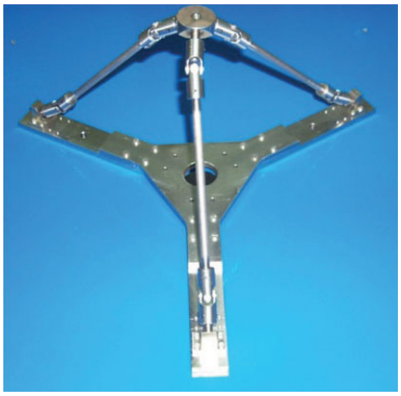

Fig. 12. (Colour online) 3-UU system using single block universal joints.

https://doi.org/10.1017/S0263574713000696 Published online by Cambridge University Press

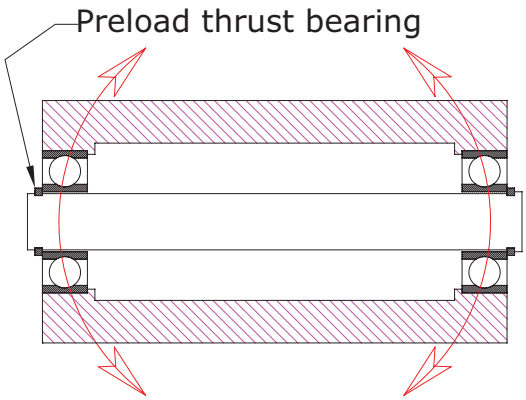

Fig. 13. (Colour online) Long bearing support with end thrust bearing preload to eliminate torsional backlash.

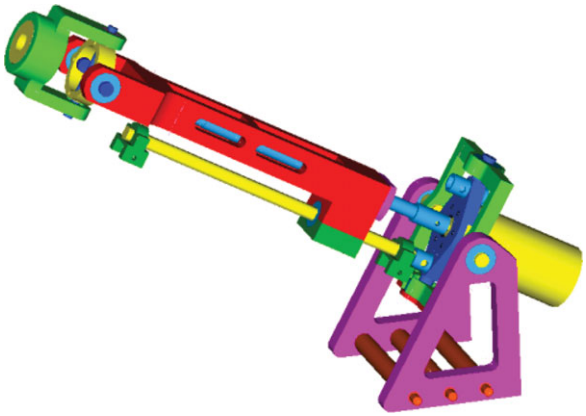

Fig. 14. (Colour online) UPU kinematic chain.

than what the maximum predicted using theoretical model.[9] The absolute sum of maximum individual errors at each joint pairs of all the legs as reported by refs. [9] and [10] gives a highly exaggerated figure and cannot be taken as a good estimate. Clearly, no disproportionate motion of the platform is observed as indicated in ref. [6]. Disproportionate motion of 3-UPU in ref. [6] is because the geometry of 3-UPU is in singularity, as also shown in ref. [8]. It was clear from the observations and the readings of the prototype model that the imprecision is due to the torsional backlash at the joints. When, we externally arrested the play partially on joints on one of the connectors, the stiffness of the platform significantly improved. The observation made in 3-UU suggests that high-precision 3-UPU is practical provided that the torsional backlash is eliminated. Instead of closely held pin hinges, distantly separated hinges would considerably reduce the torsional backlash. Also, instead of a pin and a bush, a high-precision, wide needle bearing will result in near-zero torsional backlash. For further reduction in backlash due to clearance, an end pre-loaded, outside thrust bearing retainers are accommodated in place as shown in the Fig. 13. After careful assessment of the theoretical model and the observations made on 3-UU prototype, the mechanical design of each revolute axis of a universal joint shown in Fig. 13 is evolved. The design used two block gimbal-type universal joints. Such prototype provided close to zero torsional backlash. The two support gimbal joints not only reduce the error in axis definition but also improve the torsional rigidity of the connector. The leg assembly is a serial chain formed by UPU joints. Prismatic joints are the other source for undesired torsional mobility. The prismatic joints (ball screw arrangement in this case) act as a cylindrical joint unless proper design steps are taken. The critical thing is to build the reference for pure prismatic motion. The seat of the universal joint designed as per the design considerations discussed above would serve as the reference plane, free of torsional mobility. Two parallel pre-loaded ball splines housed in the reference seat serve as the guides for pure prismatic motion. The arrangement of two pre-loaded ball splines increases the torsional rigidity and eliminates angular backlash. Figure 14 shows the near-zero backlash UPU chain.

https://doi.org/10.1017/S0263574713000696 Published online by Cambridge University Press

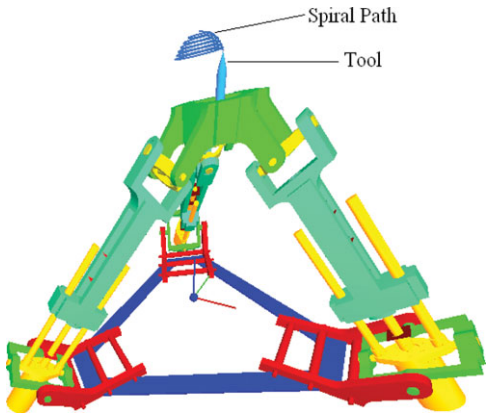

Fig. 15. (Colour online) 3D motion simulation.

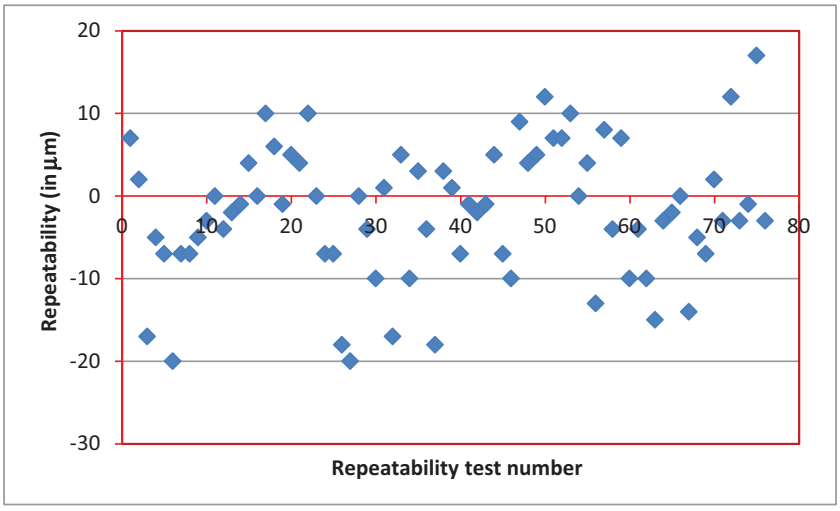

Fig. 16. (Colour online) Precision test of the prototype manipulator.

Prior to the prototype development, workspace analysis and 3D motion simulation of the 3-UPU parallel manipulator are carried out to ensure its interference-free mobility and trajectory planning throughout its motion. A software module is developed which takes the desired translations as input; the OpenGL software model shows the sequence of all the translations. The software model is used for checking feasibility of the various trajectories in the workspace. Based on the manipulator parameters and selection of the prismatic joints, the translation workspace of the manipulator is determined. Figure 15 shows the software simulation snapshot and workspace of the manipulator. Based on the design solution, a 3-DOF SPKM is developed. Each kinematic chain (see Fig. 14) consists of a DC motor integrated with an encoder of resolution 4000 counts per turn coupled to a ball screw having a lead of 1 mm. This arrangement provides high control resolution along the prismatic motion to the legs of the 3-UPU parallel manipulator. The translation range of the mechanism along the Z axis is $0 \leq z \leq 130$ mm. The translation range along the X and Y axes is $-52 \leq x \leq 79$ mm and $-69 \leq y \leq 69$ mm at different values of z.

Experiments are conducted to measure the repeatability and trajectory following accuracy for various payloads. The repeatability in achieving a position along the X, Y and Z axes is measured individually using a high-precision millitron gauge arrangement. The manipulator is given an input along each axis to reach a pre-defined position several times. The deviation of the readings among itself is recorded by using millitron gauge arrangement. The precision distribution graph shown in Fig. 16 for the number of tests of the prototype manipulator clearly demonstrates high precision. Most of the test results are within $\pm$ 10 μm.

https://doi.org/10.1017/S0263574713000696 Published online by Cambridge University Press

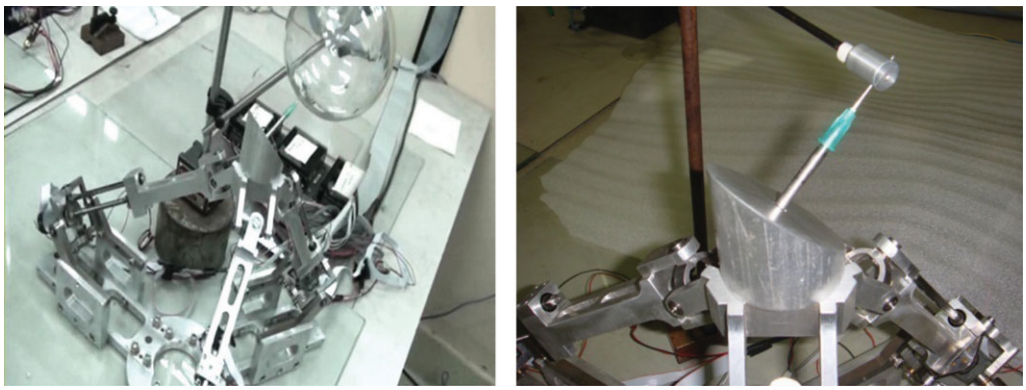

Fig. 17. (Colour online) Spatial parallel manipulator performing a high-precision job.

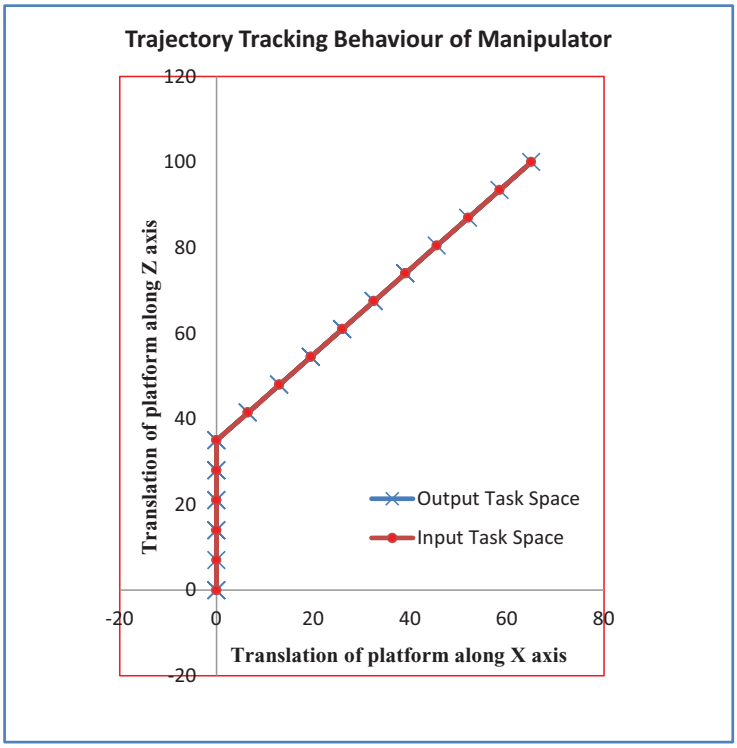

Fig. 18. (Colour online) Trajectory tracking behaviour of spatial parallel manipulator.

Figure 17 shows the prototype of the 3-DOF spatial parallel manipulator performing a high-precision job of inserting a 0.8-mm-thick needle in a 1 mm hole. Experimental analysis shows the accuracy of the manipulator to be within 30 μm. The trajectory tracking behaviour during the experiment is shown in Fig. 18. It can be observed that the trajectory following accuracy of the manipulator is very high.

The experiment to measure the accuracy of the manipulator is performed by comparing the actual paths recorded on a plane paper. The paths include some standard geometrical shapes like circle, square, rectangle, triangle and concentric circles. The actual shape of the path is compared with the values of the input path using a profile projector to determine the accuracy. The input and output data show that the trajectory following accuracy is within 30 μm.

https://doi.org/10.1017/S0263574713000696 Published online by Cambridge University Press

6. Conclusion

The paper presents result based on prototype development and validates the design. The results are in contrast to the results presented in ref. [6] for the similar three-axis translational parallel manipulator. We did not observe the prototype exhibiting any unexpected gross motion as reported in ref. [6]. We attribute the uncontrolled gross motion not to the extreme sensitivities of the mechanism to the clearance instead to the improper kinematic design considerations. The analysis and experiments confirm that the mechanism preserves the in-parallel property and it largely benefits the positional error reduction at the platform. The absolute sum of maximum individual errors at each joint pairs of all the legs as reported by refs. [9] and [10] gives a highly exaggerated figure and cannot be taken as a good estimate. Also, the synthesis shows that the Tsai 3-UPU does not suffer from disproportionate sensitivity in its workspace and the workspace boundary is farthest from the singularity surfaces. The manipulator is shown to exhibit excellent, highly repeatable trajectory following capability. This paper provides a design solution and has shown that all the merits of a parallel mechanism can be kept intact.

References

1. L.-W. Tsai and S. Joshi, "Kinematics and optimization of a spatial 3-UPU parallel manipulator," *J. Mech. Des.* **122**, 439–446 (2000).
2. S. Joshi and L.-W. Tsai, "Jacobian analysis of limited-DOF parallel manipulators," *J. Mech. Des.* **124**, 254–258 (2002).
3. B. Hu and Y. Lu, "Solving stiffness and deformation of a 3-UPU parallel manipulator with one translation and two rotations," *Robotica* **29**, 815–822 (2011).
4. R. Di Gregori and V. Parenti-Castelli, "A translational 3-DOF parallel manipulator," **In**: *Advances in Robot Kinematics: Analysis and Control* (J. Lenarcic and M. L. Husty, eds.) (Kluwer Academic Publishers, Netherlands, 1998) pp. 49–58.
5. R. Di Gregorio, V. Parenti-Castelli, "Mobility analysis of the 3-UPU parallel mechanism assembled for a pure translational motion," *J. Mech. Des.* **124**(2), 259–264 (2002).
6. C. Han, J. Kim, J. Kim and F. C. Park, "Kinematic sensitivity analysis of the 3-UPU parallel mechanism," *Mech. Mach. Theory* **37**, 787–798 (2002).
7. J. P. Merlet, "Jacobian, manipulability, condition number, and accuracy of parallel robots," *J. Mech. Des.* **128**(1), 199–206 (2005).
8. D. R. Walter, M. L. Husty and M. Pfurner, "A Complete Kinematic Analysis of the SNU 3-UPU Parallel Manipulator," **In**: *Interactions of Classical and Numerical Algebraic Geometry*, Contemporary Mathematics, vol. 496 (D. J. Bates, G. M. Besana, S. Di Rocco and C. W. Wampler, eds.) (American Mathematical Society, Providence, RI, 2009) pp. 331–346.
9. S. Venanzi and V. Parenti-Castelli, "A new technique for clearance influence analysis in spatial mechanisms," *J. Mech. Des.* **127**(5), 446–455 (2004).
10. J. Meng, D. Zhang and Z. Li, "Accuracy analysis of parallel manipulators with joint clearance," *J. Mech. Des.* **131**(1), 1–9 (2008).
11. C. Gosselin, J. Angeles, "Singularity analysis of closed-loop kinematic chains," *IEEE Trans. Robot. Autom.* **6**(3), 281–290 (1990).
12. D. L. Blanding, *Exact Constraint: Machine Design Using Kinematic Principles* (ASME Press, New York, 1999).